6 Simulations for the $K^+\Lambda$ and $K^+\Sigma^0$ Final States

6.1 K^+Y Event Generators

The $ep \rightarrow e'K^+Y$ event generators are based on model cross section calculations. The models for the $K^+\Lambda$ [12] and for the $K^+\Sigma^0$ [58] channels describe KY electroproduction in the framework of a Regge-plus-resonance approach. The resonance contributions in the s-channel are described with the help of the effective-Lagrangian approach and the background part of the amplitude is modeled in terms of t-channel Regge-trajectory exchange.

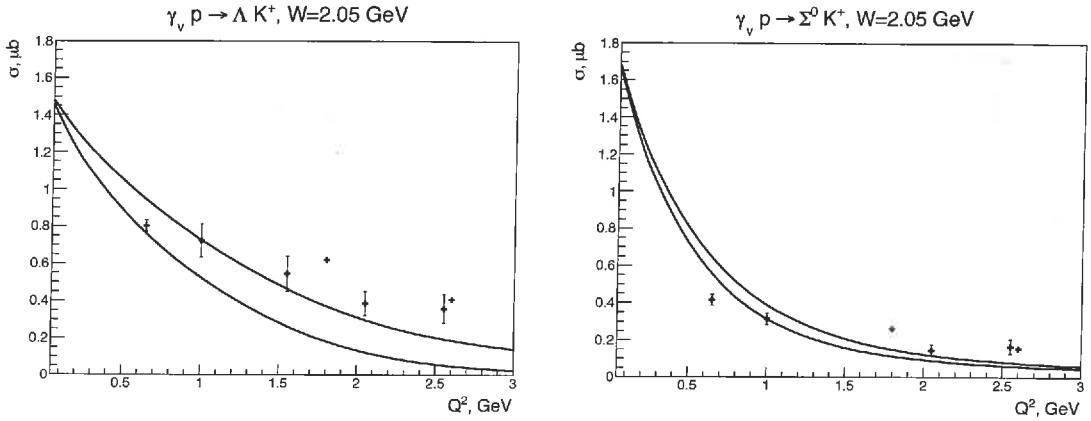

Figure 24: Integrated cross section for $K^+\Lambda$ (left) and $K^+\Sigma^0$ (right) from CLAS measurements as a function of Q^2 at $W = 2.05$ GeV [62, 64]. The cross sections at $Q^2 = 0.65$ GeV^2 are measured at a beam energy of 2.567 GeV and the cross sections at $Q^2 = 1.8$ GeV^2 and 2.6 GeV^2 are measured at a beam energy of 5.5 GeV. All other Q^2 points correspond to a beam energy of 4.056 GeV. The RPR model calculations [12, 58] are shown for E_b=2.567 GeV (upper curve) and E_b=5.5 GeV (lower curve).

A comparison of the fully integrated model cross section with experimental CLAS data is shown in Fig. 24. The cross sections are presented as a function of Q^2 for a given W bin at $W = 2.05$ GeV. The differential cross sections for representative bins of Q^2 and W are shown in Figs. 25 and 26. The model reproduces the experimental data for 0.65 $GeV^2 < Q^2 < 1.5$ GeV^2, while it considerably underestimates the cross section for $Q^2 > 1.5$ GeV^2. This underestimation is especially notable in the $K^+\Sigma^0$ channel for high Q^2 and low W. This discrepancy is not a serious concern since our kinematic region of interest is at low Q^2. However, we do have to rely on a model for the cross section as there are no experimental data available below Q^2=0.65 GeV^2 with which to compare. We can see in Figs. 25 and 26 that the model reproduces well the general features of the sharp cross section growth at large $\cos\theta_K$ for $Q^2 > 1.5$ GeV^2 and $W > 2.0$ GeV. The data included in Figs. 25 and 26 are from the CLAS measurements from Refs. [62, 64]. The Regge-plus-Resonance (RPR) model version shown included here are known as the RPR-2011 variant for the $K^+\Lambda$ final state and the RPR-2007 variant for the $K^+\Sigma^0$ final state. Further detailed comparisons of these models to the available data from CLAS for the differential cross sections, separated structure functions, and induced and transferred polarizations are given in Refs. [60, 61, 62, 63, 64].

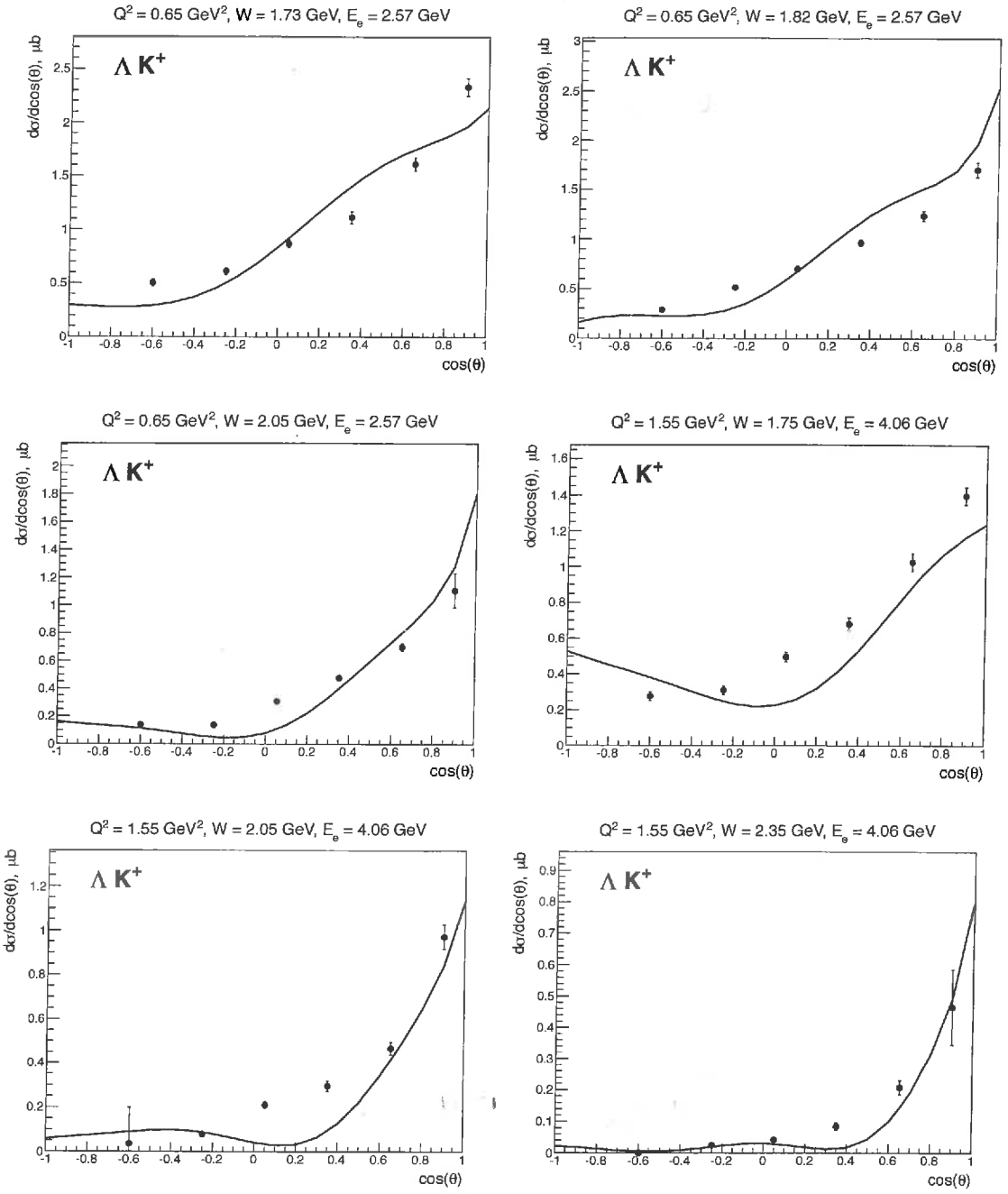

Figure 25: Differential cross sections for the $K^+\Lambda$ channel as a function of $\cos\theta_K$ from CLAS measurements in various Q^2 and W bins for two beam energies (E_b=2.57 GeV and 4.06 GeV) [62, 64] compared to the RPR model predictions (RPR-2011 variant) [12].

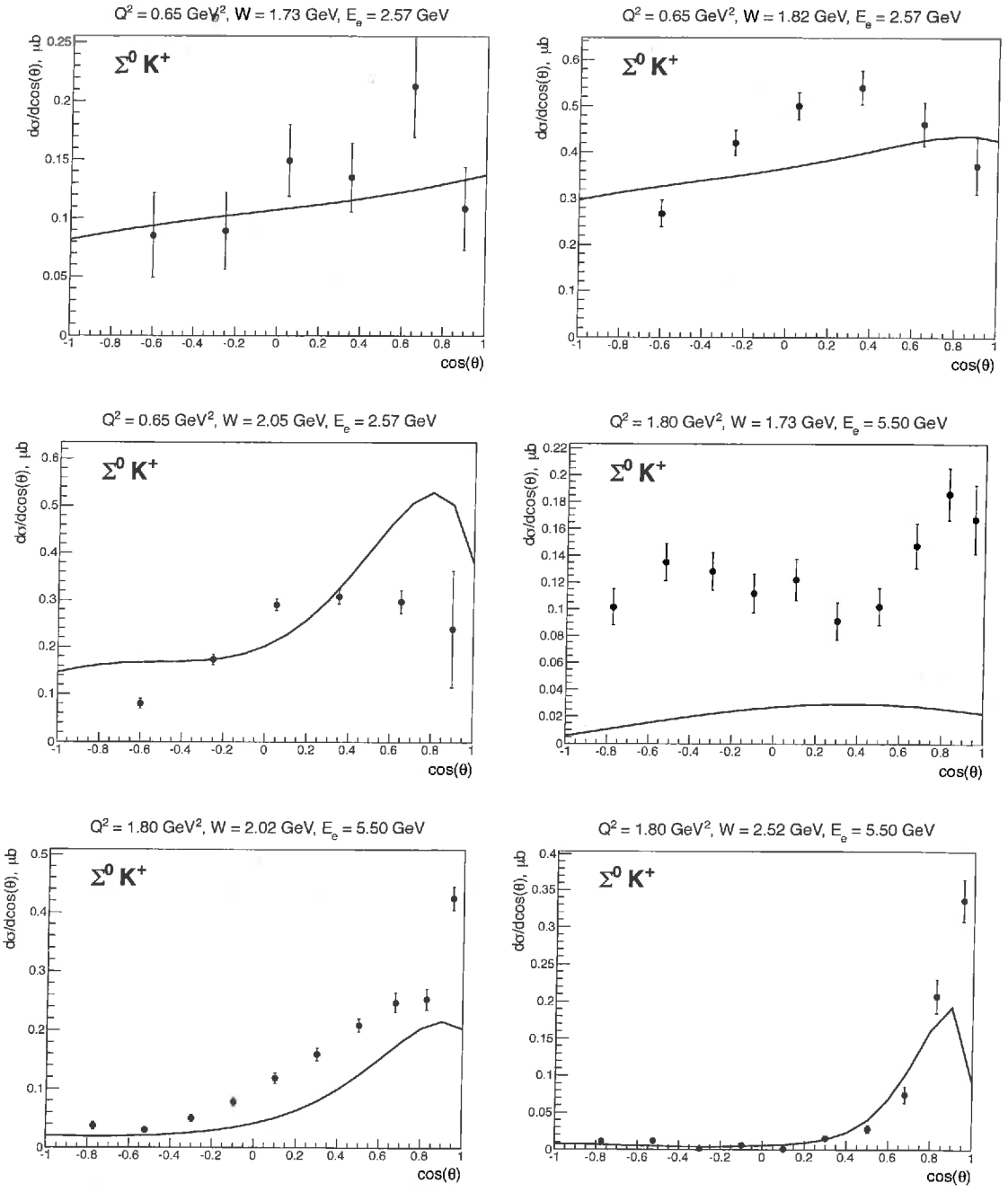

Figure 26: Differential cross sections for for $K^+\Sigma^0$ channel as a function of $\cos\theta_K$ from CLAS measurements in various Q^2 and W bins for two beam energies (E_b=2.57 GeV and 5.5 GeV). [62, 64] compared to the RPR model predictions (RPR-2007 variant) [58].

6.2 Acceptances for $ep \to e'K^+\Lambda$

In Figs. 27 and 28 we compare the angular distributions of all final states particles for an electron beam of 6.6 GeV and for torus currents of $I = +3375$ A and $I = -3375$ A. In Fig. 27 we see qualitatively the same behavior as for the $p\pi^+\pi^-$ final state; outbending electrons are generated in a W interval from $K^+\Lambda$ threshold at 1.6 GeV to 3.5 GeV and scattering angles $\theta_e \geq 2°$ are detected in CLAS12 starting at about 5° with the acceptance opening up toward larger scattering angles. The twisting pattern seen in the accepted p and K^+ plots is due to the azimuthal motion of charged tracks in the strong central solenoid field that generates a "kick" in azimuth that depends on the production angle and the particle momentum. It should be noted that the particles are not traversing the sectors in this pattern, as the plotted quantities are the values at the production vertex. The pattern for the π^- is different as they have on average much lower momenta and their migration in ϕ is larger and more diffuse.

For KY production off hydrogen, the recoil protons are kinematically limited to polar angles of $\leq 65°$. Figure 28 shows the acceptances for outbending electrons for which the polar angle gap between the FT and the CLAS12 Forward Detector calorimeters is strongly reduced and the azimuthal response is more uniform. As a result, the event acceptance for this configuration is almost a factor of two larger than for the inbending field configuration. We also note that for both configurations there exists a polar-angle band at $\theta \approx 35°$ where the acceptance is depleted due to the partially blind transition region between the Forward and Central Detector systems.

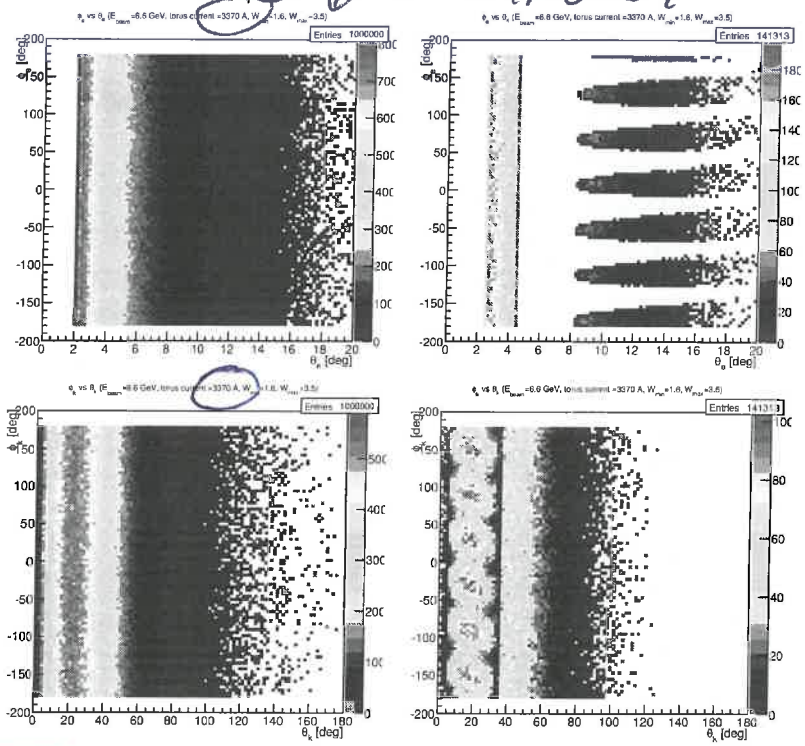

Figure 27: **(Add missing figures)** Azimuthal versus polar angle of generated (left) and accepted events (right) for electrons (top row), K^+ (2nd row), protons (third row), and π^- (bottom row). Events are generated for an electron beam energy of 6.6 GeV in a W range from 1.6 GeV to 3.5 GeV. The torus current is set I=+1500 A, that bends negatively charged particles inward towards the beamline and reduces the acceptance for electrons within CLAS12.

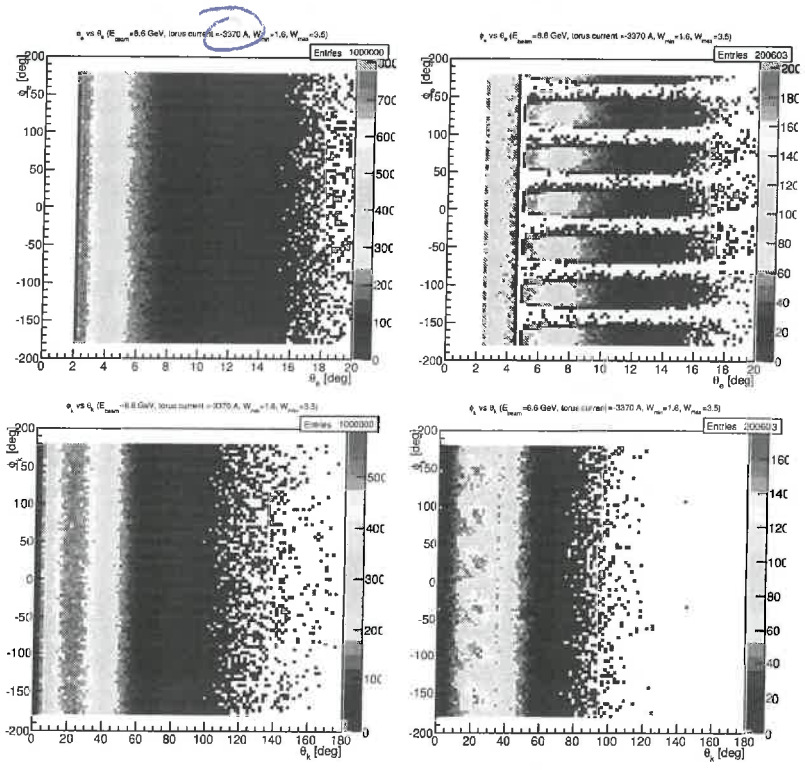

Figure 28: **(Add missing figures)** Azimuthal versus polar angles of generated (left) and accepted events (right) for electrons (top row), K^+ (2nd row), protons (third row), and π^- (bottom row). Events are generated for an electron beam energy of 6.6 GeV in a W range from 1.6 GeV to 3.5 GeV. The torus current is set at I=-1500 A, that causes negatively charged particles to bend outwards.

6.3 Run Conditions

We are planning to search for hybrid states at low Q^2 and the accessible range of Q^2 depends on the beam energy and torus current. Another issue that affects the selection of the best run condition is that we need good particle momentum resolution to be able to separate the $K^+\Lambda$ and $K^+\Sigma^0$ electroproduction channels and the best resolution is achieved with larger torus currents. The $K^+\Lambda$ and $K^+\Sigma^0$ channel separation is based on missing mass cuts on the reconstructed $e'K^+$ missing mass. For this purpose the final state K^+ must be detected. Thus, we have to use exclusive topologies where the final state electron, the K^+ and at least one of the other hadrons (p or π^-) are detected. The detection of the decay p or π^- from the Λ decay is required in order to measure the induced and transferred polarizations of the hyperons. Measurements of these hyperon polarization components from CLAS data are given in Refs. [59, 60].

The run condition studies were performed with the CLAS12 FASTMC program. Table 2 summarizes the minimum Q^2 coverage for the K^+Y final states at E_b=6.6 GeV and 8.8 GeV for different torus field settings and polarities. As already mentioned in Section 4.3, the optimal running conditions correspond to data collection with large negative torus current, where the maximal $K^+\Lambda$ and $K^+\Sigma^0$ separation is achieved and the gap in the Q^2 coverage between the FT and the CLAS12 Forward Detector calorimeters is the smallest. Studies of the reconstructed $e'K^+$ missing mass combining the data for the $K^+\Lambda$ and $K^+\Sigma^0$ channels for different torus field/polarity conditions are shown in Figs. 29 and 30. Clearly the data collection at the highest possible torus field settings, corresponding to the best charged particle momentum resolution, is optimal for separation of the KY reaction channels.

E_b, GeV	Tor. current, A	Q^2_{min}, GeV^2
6.6	+1500	0.05
6.6	−1500	0.05
6.6	+3700	0.05
6.6	**−3375**	0.05
8.8	+1500	0.1
8.8	−1500	0.1
8.8	+3700	0.1
8.8	**−3375**	0.1

Table 2: Minimal achievable Q^2 (Q^2_{min}) for different torus currents and polarities at E_b=6.6 GeV and 8.8 GeV for the $K^+\Lambda$ and $K^+\Sigma^0$ final states.

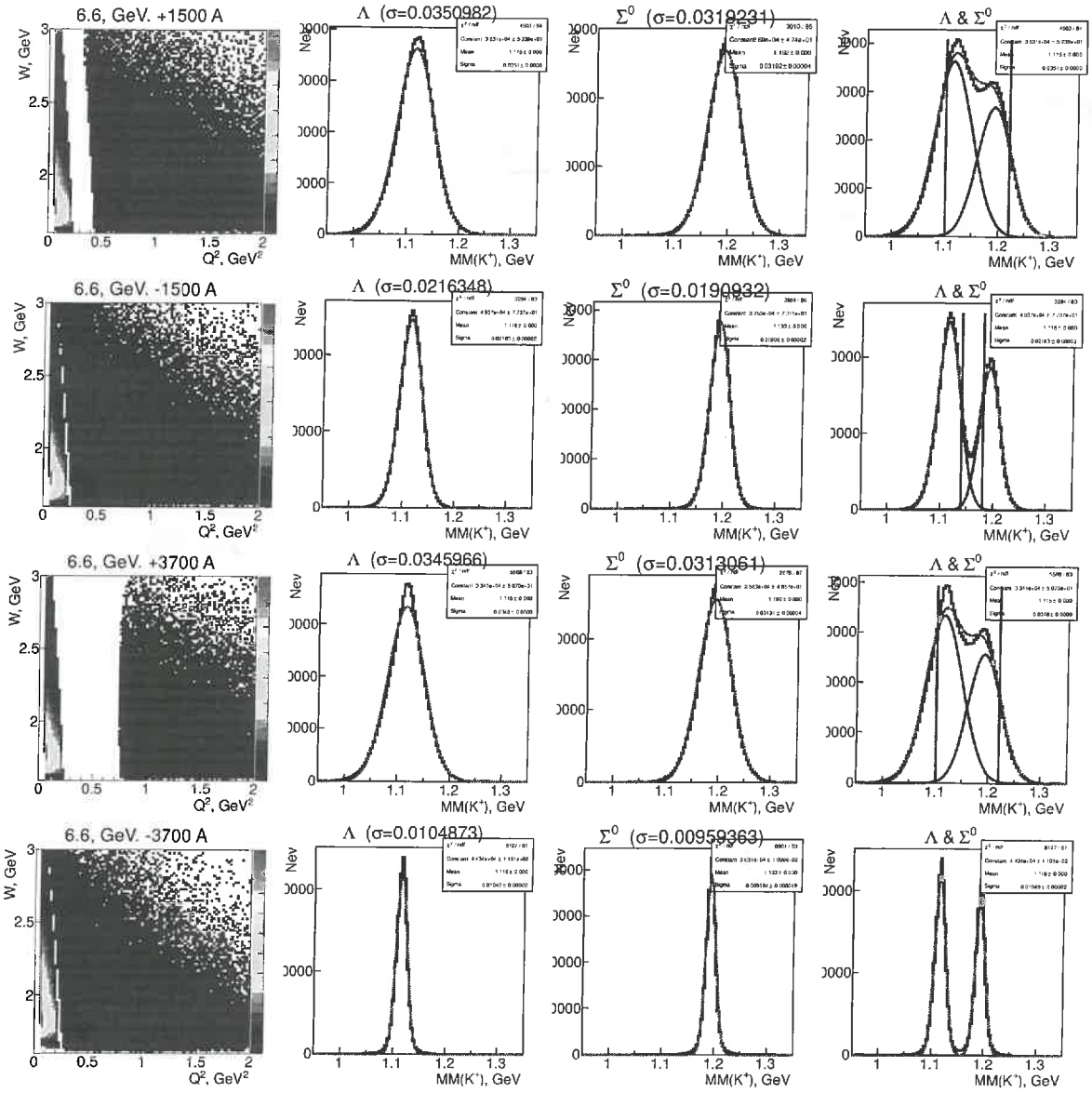

Figure 29: The left column shows the W versus Q^2 distributions at different torus currents for $Q^2 < 2$ GeV^2 for E_b=6.6 GeV. The next three columns show the distributions of the $e'K^+$ missing mass for the different torus currents. The right column shows the combined $K^+\Lambda$ and $K^+\Sigma^0$ overlaps (no background included) to demonstrate the requirement to take data at the highest possible CLAS12 torus setting.

6.4 Count Rates for $K^+\Lambda$

The expected total number of K^+Y electroproduction events in the reaction $ep \to e'K^+Y$ can be written as:

$$N = \mathcal{L} \cdot t \cdot \int \frac{d^5\sigma}{dE_e d\Omega_e d\Omega_K} dE_e d\Omega_e d\Omega_K, \tag{1}$$

where

- $\mathcal{L} = 1 \times 10^{35}$ cm^{-2}s^{-1} is the expected CLAS12 operating luminosity
- t is the expected run time, and
- $\frac{d^5\sigma}{dE_e d\Omega_e d\Omega_K}$ is the cross section from Eq.(21).

The integration in Eq.(1) is performed over the entire kinematic space and the event rate R is defined as $\frac{N}{t}$.

The integration in Eq.(1) can be done numerically. We use the same model cross sections for $d^2\sigma/d\Omega_K^*$ as was used in the event generator (see Section 6.1). The minimum achievable value of Q^2 in CLAS12 is determined by the forward hole, where high energy electrons cannot be detected. For all beam energies Q^2 is greater than 0.01 GeV^2, so we can integrate in Eq.(1) given that $Q^2 > 0.01$ GeV^2. The calculated event rates R_Λ and R_{Σ^0} are presented in Table 3.

E_{beam}, GeV	R_Λ, Hz	R_{Σ^0}, Hz
6.6	1500	1200
8.8	1400	1100

Table 3: Estimated production rates for events with $Q^2 > 0.01$ GeV^2.

To account for the acceptance of CLAS12, a detailed simulation is needed. As we need to generate events in the entire kinematic space with $Q^2 > 0.01$ GeV^2, the ratio of reconstructed to generated events gives the averaged acceptance. Multiplying the event rates from Table 3 by that ratio, we obtain the event rates that account for the CLAS12 acceptance. An $ep \to e'K^+\Lambda \to e'K^+p\pi^-$ event is considered to be reconstructed if the electron and at least two hadrons have been detected. A trigger condition requiring at least two charged hadrons and an electron would select our channels of interest.

The accepted event rate calculations are presented in Table 4 for different torus currents and polarities for E_b=6.6 GeV and 8.8 GeV, taking into account the branching ratio for the Λ decay into $p\pi^-$ (64%). A rough estimate suggests that the KY exclusive channel contribution is about 1% with respect to the two and three pion events, which are expected to dominate the events that have an electron and at least two charged hadrons in the final state. The maximal total event rate is therefore expected to be $\approx$ 25 kHz for the trigger condition described above. This estimate is compatible with the following considerations: suppose that the maximal inclusive event rate is 20 kHz, which is limited by the data acquisition. Then under the rough assumption that the $K^+\Lambda$ event rate is about 1% with respect to the inclusive event rate, we can estimate the $K^+\Lambda$ event rate to be $\approx$ 128 Hz. This number is in a reasonable agreement with the previously obtained value of 144 Hz.

E_{beam}, GeV	Torus Current A	R_Λ, Hz
6.6	+1500	144
6.6	-1500	154
6.6	+2950	87
6.6	-2950	72
8.8	+1500	108
8.8	-1500	108
8.8	+2950	67
8.8	-2950	52

Table 4: Estimated event rates for the $ep \to e'K^+\Lambda \to e'K^+p\pi^-$ channel, where the electron and two hadrons are required to be detected.

6.5 Expected K^+Y Total Event Rates

At the very forward electron scattering angles, electron rates will be very high and may exceed the capabilities of the data acquisition system. Therefore additional constraints are needed to define an optimal trigger configuration to enrich the sample with final state topologies that might be expected for the hybrid baryon candidates and to reduce the total acquisition rate. For our initial running program, we therefore consider a trigger for the hadronic final states with at least two charged particles. This will cover final states like $K^+\Lambda \to K^+p\pi^-$, $p\pi^+\pi^-$, $p\phi \to pK^+K^-$, and $p\eta' \to p\pi^+\pi^-\eta$. For realistic rate estimates, projections of the hadronic coupling strengths of the hybrid baryons are needed, which are currently not available. In addition, a single charged hadron trigger will be incorporated with a pre-scaling factor for the FT, which in parallel will collect events with a single charged hadron in the final state, i.e. π^+n, $p\pi^0$, $K^+\Lambda$, and $K^+\Lambda$, among others.

The nominal operating luminosity of CLAS12 is expected to be $\mathcal{L} = 1 \times 10^{35}$ cm^{-2}sec^{-1}. This corresponds to a production rate of 70 Hz (for $K^+\Lambda$) and about 50 Hz (for $K^+\Sigma^0$). For a 30 day run at the nominal luminosity, the total number of $K^+\Lambda$ events is estimated to be 1.8×10^8 and the number of $K^+\Sigma^0$ events to be 1.3×10^8. The lowest event rate is expected for high Q^2 and high W. For the kinematics with lowest statistics, e.g. $2.0 \le Q^2 \le 2.5$ GeV^2 and $2.675 \le W \le 2.700$ GeV, a total number of 2.0×10^5 $K^+\Lambda$ events and 1.1×10^5 $K^+\Sigma^0$ events is expected.

While these rates seem very large, it should be kept in mind that the signals of the hybrid baryons that we want to detect and quantify may be one or two orders of magnitude smaller than the signal from ordinary baryon states and will likely not simply be seen as a peak in the excitation spectrum, but rather as a broad region in W, where specific quantum numbers, i.e. $I = \frac{1}{2}$ and $J^P = \frac{1}{2}^+$ or $J^P = \frac{3}{2}^+$, must be identified and the electromagnetic couplings must be measured versus Q^2. This can be achieved in a partial-wave analysis that includes other channels in a multichannel fit, such as the Bonn-Gatchina or Jülich/GWU approaches. Other techniques may also be employed. This high statistics is thus essential, and the transverse and longitudinal photon polarization that is inherent in electron scattering will provide amplitude interference that could be expected to enhance the resonant signal.